



LJMU Research Online

Parker, RJ

Dynamics versus structure: breaking the density degeneracy in star formation

<http://researchonline.ljmu.ac.uk/id/eprint/1487/>

Article

Citation (please note it is advisable to refer to the publisher's version if you intend to cite from this work)

Parker, RJ (2014) Dynamics versus structure: breaking the density degeneracy in star formation. Monthly Notices of the Royal Astronomical Society, 445 (4). pp. 4037-4044. ISSN 0035-8711

LJMU has developed **LJMU Research Online** for users to access the research output of the University more effectively. Copyright © and Moral Rights for the papers on this site are retained by the individual authors and/or other copyright owners. Users may download and/or print one copy of any article(s) in LJMU Research Online to facilitate their private study or for non-commercial research. You may not engage in further distribution of the material or use it for any profit-making activities or any commercial gain.

The version presented here may differ from the published version or from the version of the record. Please see the repository URL above for details on accessing the published version and note that access may require a subscription.

For more information please contact researchonline@ljmu.ac.uk

<http://researchonline.ljmu.ac.uk/>

Dynamics versus structure: breaking the density degeneracy in star formation

Richard J. Parker^{*}

Astrophysics Research Institute, Liverpool John Moores University, 146 Brownlow Hill, Liverpool, L3 5RF, UK

ABSTRACT

The initial density of individual star-forming regions (and by extension the birth environment of planetary systems) is difficult to constrain due to the “density degeneracy problem”: an initially dense region expands faster than a more quiescent region due to two-body relaxation and so two regions with the same observed present-day density may have had very different initial densities. We constrain the initial densities of seven nearby star-forming regions by folding in information on their spatial structure from the Q -parameter and comparing the structure and present-day density to the results of N -body simulations. This in turn places strong constraints on the possible effects of dynamical interactions and radiation fields from massive stars on multiple systems and protoplanetary discs.

We apply our method to constrain the initial binary population in each of these seven regions and show that the populations in only three – the Orion Nebula Cluster, ρ Oph and Corona Australis – are consistent with having evolved from the Kroupa universal initial period distribution and a binary fraction of unity.

Key words: stars: formation – planetary systems – open clusters and associations – methods: numerical – binaries: general

1 INTRODUCTION

Characterising the formation environment of stars is one of the outstanding challenges in astrophysics. If stars are predominately born in dense ‘clustered’ environments (e.g. Lada & Lada 2003; Lada 2010) then dynamical interactions and the radiation fields from massive stars may significantly affect the formation and evolution of planetary systems (e.g. Armitage 2000; Bonnell et al. 2001; Scally & Clarke 2001; Adams et al. 2006; Olczak et al. 2008; Parker & Quanz 2012; Rosotti et al. 2014) and the properties of binary and multiple systems (e.g. Kroupa 1995a; Kroupa et al. 1999; Marks & Kroupa 2012; Parker & Goodwin 2012).

On the other hand, if most stars are born in relative isolation (e.g. Shu, Adams & Lizano 1987), or rather in low-density environments where dynamical interactions are insignificant (e.g. Bressert et al. 2010), then planetary and binary systems may form with little or no external perturbation. Either scenario has important implications for understanding the origin of stars in the Galactic field, and for placing our Solar System in the context of exoplanetary systems (e.g. Adams 2011; Alexander et al. 2013; Davies et al. 2013, and references therein).

Ideally, we would like to compare the properties of observed star-forming regions and young clusters to simulations to gauge the effects of the star-forming environment on binary systems and fledgling planetary systems. Binary systems are particularly useful

because their properties in the Galactic field are well-constrained (Raghavan et al. 2010; Duchêne & Kraus 2013). In principle one can compare binary populations between star-forming regions and the Galactic field, in order to determine the type of star-forming region that produces the most ‘field-like’ binaries (and hence is the dominant star-forming event that produces the Galactic field; Goodwin 2010).

Unfortunately, this problem is severely complicated by uncertainty in determining the maximum density attained by star-forming regions. Observations of the present-day density in star-forming regions provide very few constraints on the initial density (e.g. King et al. 2012a; Moeckel et al. 2012; Gieles et al. 2012; Parker & Meyer 2012). The reason is that an initially dense region expands very quickly due to two-body relaxation, whereas a less dense region expands more slowly. Therefore, at a given age two regions with the same present-day density may have had very different densities in the past. This is the so-called “density degeneracy problem” – not enough information is available to rule out much more dense initial conditions (e.g. Marks & Kroupa 2012; Marks et al. 2014).

In this paper, we attempt to address this issue by folding in extra information on the structure of star forming regions (Cartwright & Whitworth 2004), and (where available) the relative density around massive stars with respect to the median stellar density in the region (Maschberger & Clarke 2011). We compare observational data for seven nearby star-forming regions to the results of N -body simulations where we vary the initial density to deter-

^{*} E-mail: R.J.Parker@ljmu.ac.uk

mine the most likely initial conditions of each region. As an example of the method, we then use these constraints to rule out the universal binary population hypothesis from Kroupa (1995a,b). We describe our simulation set-up in Section 2, we present our results in Section 3 and we conclude in Section 4.

2 METHOD

2.1 Star-forming region set-up

Both observations (e.g. Cartwright & Whitworth 2004; Sánchez & Alfaro 2009; Gouliermis et al. 2014) and simulations (Schmeja & Klessen 2006; Girichidis et al. 2012; Dale et al. 2013) of star-forming regions indicate that stars form with a hierarchical, or self-similar spatial distribution (i.e. they are substructured). It is almost impossible to create substructure through dynamical interactions; rather it is usually completely erased over a few crossing times (Parker et al. 2014). Therefore, in order to reproduce the substructure observed in many of the regions of interest here, we must start the simulations with substructure.

We set up substructured star forming regions using fractal distributions, following the method of Goodwin & Whitworth (2004). This method is described in detail in that paper, and in Allison et al. (2010) and Parker et al. (2014). Briefly, the fractal is built by creating a cube containing ‘parents’, which spawn a number of ‘children’ depending on the desired fractal dimension. The amount of substructure is then set by the number of children that are allowed to mature. The lower the fractal dimension, the fewer children are allowed to mature and the cube has more substructure. Fractal dimensions in the range $D = 1.6$ (highly substructured) to $D = 3.0$ (uniform distribution) are allowed. Finally, outlying particles are removed so that the cube from which the fractal was created becomes a sphere; however, the distribution is only truly spherical if $D = 3.0$.

All of our simulated star-forming regions have a fractal dimension $D = 1.6$; the Taurus association (Cartwright & Whitworth 2004) and Corona Australis (CrA, Neuhäuser & Forbrich 2008) both have fractal dimensions consistent with this value and because dynamical interactions cannot make a region more substructured, we adopt this value. However, we note that hydrodynamical simulations of star formation can produce less substructured regions (higher D values) and as we shall see, some observed regions must also have higher primordial fractal dimensions.

The velocities of stars in the fractals are also correlated on local scales, in accordance with observations (Larson 1982; André et al. 2010). The children in our fractals inherit their parents’ velocity, plus a small amount of noise which successively decreases further down the fractal tree. This means that two nearby stars have very similar velocities, whereas two stars which are distant can have very different velocities. Again, this is an effort to mimic the observations of star formation, which indicate that stars in filaments have very low velocity dispersions (André et al. 2010).

In order to erase primordial substructure and to process primordial binary systems as efficiently as possible, we scale the velocities of the whole fractal to be subvirial ($\alpha_{\text{vir}} = 0.3$, where the virial ratio $\alpha_{\text{vir}} = T/|\Omega|$; T and Ω are the total kinetic energy and total potential energy of the stars, respectively).

We set up our star-forming regions with three different densities. In two sets of simulations, the regions have a radius of 1 pc and contain either 1500 stars (which we will refer to as “high density” – $\bar{\rho} \sim 10^4 M_{\odot} \text{pc}^{-3}$) or 150 stars (“medium density” – $\bar{\rho} \sim$

$10^2 M_{\odot} \text{pc}^{-3}$). In a third set of simulations, the regions contain 300 stars and have a radius of 5 pc (“low density” – $\bar{\rho} \sim 10 M_{\odot} \text{pc}^{-3}$).

2.2 Binary population

All of our regions have an initial binary fraction of unity, i.e. everything forms in a binary. When creating the binary populations we adopt the same initial conditions as in Marks et al. (2014). The primary masses are drawn from a Kroupa (2002) IMF of the form

$$\frac{dN}{dM} \propto \begin{cases} M^{-1.3} & m_0 < M/M_{\odot} \leq m_1, \\ M^{-2.3} & m_1 < M/M_{\odot} \leq m_2, \end{cases} \quad (1)$$

where $m_0 = 0.1 M_{\odot}$, $m_1 = 0.5 M_{\odot}$, and $m_2 = 50 M_{\odot}$, clusters. There are no brown dwarfs in the simulations. Secondary masses are also drawn at random from the IMF; note this is inconsistent with recent observations (Metchev & Hillenbrand 2009; Reggiani & Meyer 2013) which show a universal flat companion mass ratio distribution. However, subsequent pre-main sequence eigenevolution (see below) alters the mass ratios of close binaries so that the CMRD approaches a flat distribution.

Binary periods are drawn from the Kroupa (1995b) period distribution (see also Kroupa & Petr-Gotzens 2011; Marks et al. 2014) of the form

$$f(\log_{10} P) = \eta \frac{\log_{10} P - \log_{10} P_{\min}}{\delta + (\log_{10} P - \log_{10} P_{\min})^2}, \quad (2)$$

where $\log_{10} P_{\min}$ is the logarithm of the minimum period in days and $\log_{10} P_{\min} = 1$. $\eta = 2.5$ and $\delta = 45$ are the numerical constants adopted by Kroupa (1995b). This period distribution was derived from a process of “reverse engineering” N -body simulations (Kroupa 1995a,b,c); regions with low densities do not break up many binaries and hence would have an excess of wide systems ($100 - 10^4$ au) compared to the Galactic field, as observed in Taurus (Leinert et al. 1993; Köhler & Leinert 1998), whereas more dense regions would destroy more wider binaries and the resultant separation distribution is more “field-like” (Duquennoy & Mayor 1991; Fischer & Marcy 1992; Raghavan et al. 2010).

Eccentricities are drawn from a thermal distribution (Heggie 1975) of the form

$$f(e) = 2e. \quad (3)$$

We note that the eccentricity distribution of binaries in the field is more consistent with a flat distribution (Raghavan et al. 2010; Duchêne & Kraus 2013); however, as with the mass ratios, eigenevolution alters the distribution for close systems.

Finally, we apply the Kroupa (1995b) ‘eigenevolution’ algorithm, which accounts for tidal circularisation effects in close binaries (Mathieu 1994), and for early angular momentum transfer between the circumprimary disk and the secondary star.

We then place the binary systems at the centre of mass of each position in the fractal and we evolve the star-forming regions for 10 Myr using the *kira* integrator in the *Starlab* package (Portegies Zwart et al. 1999, 2001). We do not include stellar evolution in the simulations.

3 RESULTS

We first demonstrate the density degeneracy and its effect on the binary properties in star-forming regions. In order to invoke a universal model of star formation and to reconcile differences between the

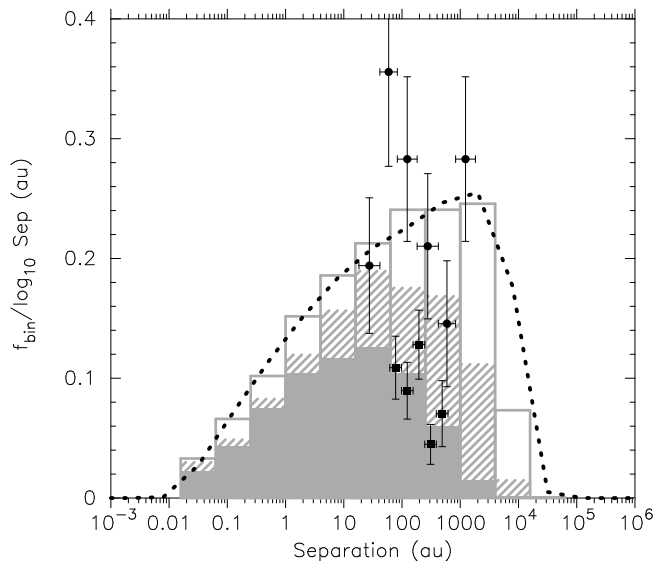


Figure 1. Evolution of the separation distribution normalised to the binary fraction as a function of initial density. The primordial distribution (Kroupa 1995b) is shown by the dotted line and the distributions after 1 Myr are shown by the open (low density – $\bar{\rho} \sim 10 M_{\odot} \text{pc}^{-3}$), hashed (medium density – $\bar{\rho} \sim 10^2 M_{\odot} \text{pc}^{-3}$) and solid (high density – $\bar{\rho} \sim 10^4 M_{\odot} \text{pc}^{-3}$) histograms. The observed distributions for Taurus (the circles, Köhler & Leinert 1998) and the Orion Nebula Cluster (the squares, Reipurth et al. 2007) are also shown.

binary populations of Taurus (Leinert et al. 1993) and the Galactic field (Duquennoy & Mayor 1991), Kroupa (1995a,b) postulated a universal initial binary population where all stars form in binaries, with an excess of systems with wide ($10^2 - 10^4$ au) semimajor axes with respect to the field population. In Fig. 1 we show the initial Kroupa (1995b) binary period distribution (Eqn. 2), converted to a separation distribution, by the dotted line. Depending on the maximum density attained by the region, the binaries can suffer none, little, or much dynamical destruction and the separation distribution is altered accordingly. We show the distribution (at 1 Myr) in the simulated low density regions by the open histogram, the distribution in the medium density regions by the hashed histogram and the distribution in the high density regions by the solid histogram. We also show the observational data points for Taurus (consistent with little dynamical evolution of the proposed initial period distribution; Köhler & Leinert 1998) by the circles and the Orion Nebula Cluster (ONC, consistent with significant dynamical evolution of the proposed initial period distribution; Reipurth et al. 2007), by the squares.

3.1 Evolution of density

If a star-forming region is older, it has had more time to process its primordial binary population (Marks & Kroupa 2012). Therefore, a 3 Myr old region can have a much lower density than a 1 Myr old region, even though they may have had the same initial density; the difference is that two-body relaxation has caused the older region to expand more over time. We show the evolution of density as a function of time in Fig. 2. In panel (a) we show the evolution of our high density ($\bar{\rho} \sim 10^4 M_{\odot} \text{pc}^{-3}$) regions, and in panel (b) we show the medium initial density ($\bar{\rho} \sim 10^2 M_{\odot} \text{pc}^{-3}$) regions. In panel (c) we show the evolution of the low-density regions ($\bar{\rho} \sim 10 M_{\odot} \text{pc}^{-3}$)

In all panels, the median density in each of our 20 simulated regions is shown by the solid grey lines.

The regions evolve to form a bound stellar cluster, and stars which are in the very centre of the cluster have higher densities than the region median (the grey lines). We show the evolution of the averaged central density (the volume density within the half-mass radius) by the dot-dashed lines. Conversely, stars that are ejected from the regions and become unbound have significantly lower densities.

In Fig. 2 we also show the current density of several nearby regions of varying ages (see the final column of Table 1 for a key to the symbols). Marks & Kroupa (2012) and Marks et al. (2014) argue that given a universal primordial binary population, limits can be placed on the primordial density of a region by comparing the outcome of N -body simulations with the currently observed visual binary population. We indicate the best-fit initial density for each region studied in Marks & Kroupa (2012) and Marks et al. (2014) by the red symbols around $t = 0$ Myr (the same symbols are used as for the present-day densities – for example, Cham I is shown by the \star). Outside of the error bars, Marks & Kroupa (2012) reject the possibility of that density being consistent with the processing of a common binary population with 90 per cent confidence.

Taking the density in isolation, Fig. 2 shows that for ρ Oph and the ONC (the filled diamonds and squares, respectively) both a high-density region which evolves to far lower densities (panel a) and a medium-density region that remains static within the first Myr (panel b) are consistent with the observations. However, when their binary populations are considered, Marks & Kroupa (2012) show that under the assumption of a universal primordial binary population, the initial densities must be more than a factor of 10 different.

3.2 Evolution of structure

In order to break this density degeneracy, we compare the evolution of the spatial structure in our simulations, as measured by the Q -parameter (Cartwright & Whitworth 2004; Cartwright & Whitworth 2009; Cartwright 2009). The Q -parameter compares the mean length of the minimum spanning tree (the shortest possible pathlength between all stars where there are no closed loops, \bar{m}) to the mean separation between stars, \bar{s} :

$$Q = \frac{\bar{m}}{\bar{s}}. \quad (4)$$

A region is substructured if $Q < 0.8$, and centrally concentrated if $Q > 0.8$. We show the evolution of Q in our simulations compared to the measured values in Fig. 3 at various ages (see Table 1 for a key to the symbols). The determination of the Q -parameter requires only positional information; however, it can be affected by extinction and membership uncertainty (Bastian et al. 2009; Parker & Meyer 2012). Where there is an uncertainty associated with the determination of Q , we show the likely direction of the uncertainty. For example, Cartwright & Whitworth (2004) determined $Q = 0.85$ for ρ Oph; however, using an updated census discussed in Alves de Oliveira et al. (2012), Parker et al. (2012) find $Q = 0.56$. In our subsequent analysis, we consider any evolutionary scenario that is consistent with either value to be plausible initial conditions for that star-forming region. Similarly, depending on membership probability, Upper Sco and CrA may have lower Q -parameters (once probable back- and foreground stars are removed), whereas the ONC likely has a higher Q -parameter than that determined from the Hillenbrand & Hartmann (1998) data due to visual extinction and sample incompleteness.

Table 1. A summary of the regions with which we compare our N -body simulations. From left to right, the columns show the region name, age, Q -parameter, an alternative determination where applicable, Q_{alt} (see text for details), the Σ_{LDR} ratio (if available), the references for Q , Q_{alt} , Σ_{LDR} , the observed present-day density of each region as noted by Marks & Kroupa (2012) and King et al. (2012b), $\rho_{\text{obs.}}$, the postulated initial density, $\rho_{\text{post.}}$, from Marks & Kroupa (2012) and Marks et al. (2014) for the binary population of that region to be consistent with the universal primordial binary properties (Kroupa 1995a), and the symbol used in Figs. 2 and 3.

Region	Age	Q	Q_{alt}	Σ_{LDR}	Refs.	$\rho_{\text{obs.}}$	$\rho_{\text{post.}}$	symbol
ONC	1 Myr	0.87	0.94	3.7	Hillenbrand & Hartmann 1998	$400 \text{ M}_{\odot} \text{ pc}^{-3}$	$68\,000 \text{ M}_{\odot} \text{ pc}^{-3}$	■
ρ Oph	1 Myr	0.85	0.56	0.58	Cartwright & Whitworth 2004; Parker et al. 2012	$200 \text{ M}_{\odot} \text{ pc}^{-3}$	$2300 \text{ M}_{\odot} \text{ pc}^{-3}$	◆
Taurus	1 Myr	0.48	–	0.28	Cartwright & Whitworth 2004; Parker et al. 2011	$8 \text{ M}_{\odot} \text{ pc}^{-3}$	$350 \text{ M}_{\odot} \text{ pc}^{-3}$	●
IC 348	3 Myr	0.92	–	–	Cartwright & Whitworth 2004	$180 \text{ M}_{\odot} \text{ pc}^{-3}$	$9400 \text{ M}_{\odot} \text{ pc}^{-3}$	◇
Cham I	3 Myr	0.66	0.71	–	Cartwright & Whitworth 2004; Cartwright & Whitworth 2009	$1 \text{ M}_{\odot} \text{ pc}^{-3}$	$1600 \text{ M}_{\odot} \text{ pc}^{-3}$	★
CrA	1 Myr	0.38	0.32	–	Neuhäuser & Forbrich 2008	$30 \text{ M}_{\odot} \text{ pc}^{-3}$	$190 \text{ M}_{\odot} \text{ pc}^{-3}$	▲
Upper Sco	5 Myr ^a	0.88	0.75	–	Kraus & Hillenbrand 2007	$16 \text{ M}_{\odot} \text{ pc}^{-3}$	$4200 \text{ M}_{\odot} \text{ pc}^{-3}$	○

^aNote that the age of Upper Sco may be as high as 11 Myr (Pecaut, Mamajek & Bubar 2012).

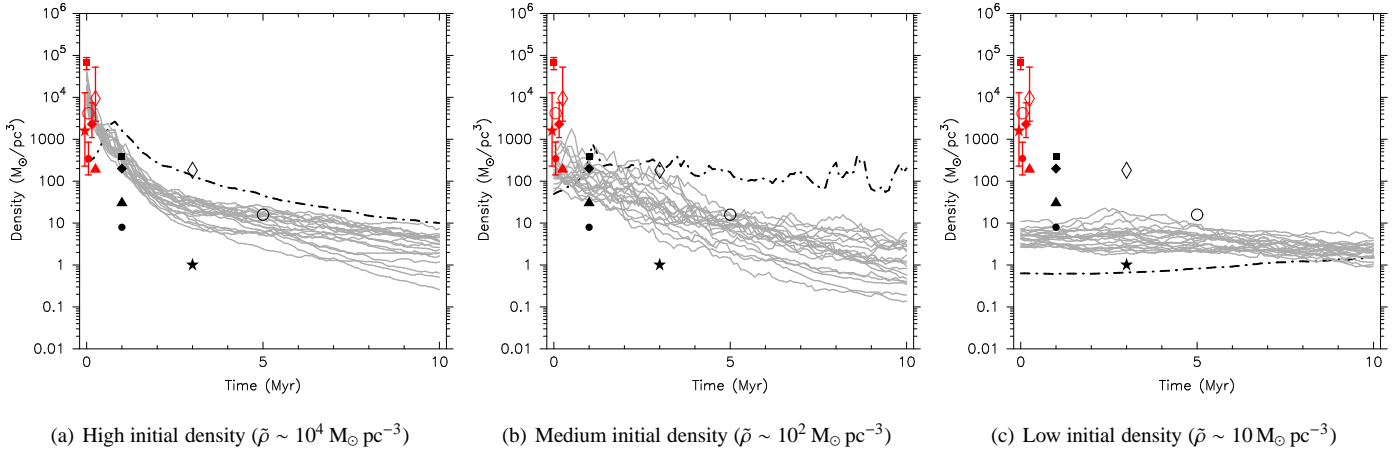


Figure 2. Evolution of the density in our simulated star-forming regions. In panel (a) the star-forming regions have high initial densities ($\bar{\rho} \sim 10^4 \text{ M}_{\odot} \text{ pc}^{-3}$), in panel (b) the regions have medium initial densities ($\bar{\rho} \sim 10^2 \text{ M}_{\odot} \text{ pc}^{-3}$) and in panel (c) the regions have much lower initial densities ($\bar{\rho} \sim 10 \text{ M}_{\odot} \text{ pc}^{-3}$). We show the median stellar volume density in each simulation by the individual grey (solid) lines, and the central density (within the half-mass radius) from twenty averaged simulations. The lefthand red symbols (at $t = 0$ Myr, slightly offset from one another for clarity) are the required initial densities for several nearby star-forming regions if star formation is consistent with a universal initial binary population (Marks & Kroupa 2012; Marks et al. 2014). The corresponding present-day stellar densities are shown by the black points at 1, 3 and 5 Myr, depending on the age of the region. A key to the symbols is provided in Table 1.

Finally, Cham I is slightly elongated, which means the true Q -parameter is slightly higher than measured (0.71 instead of 0.66, Cartwright & Whitworth 2009). These ‘alternative’ measurements are shown in column 4 of Table 1 (Q_{alt}).

As in Fig. 2, panel (a) shows the simulations with initially high densities, panel (b) shows the medium density simulations and panel (c) shows the low density simulations. The solid grey lines are the individual simulations, and the horizontal red dashed line shows the boundary between substructured regions ($Q < 0.8$) and centrally concentrated regions ($Q > 0.8$).

We exclude unbound stars from the determination of Q for two reasons. Firstly, Q can appear artificially high when distant stars are included in the analysis, and secondly, stars that are unbound in the simulations are likely to travel far from the regions very quickly, making the comparison with observations unfair.

As pointed out in Parker & Meyer (2012) and Parker et al. (2014), the more dense a region is initially, the more readily substructure is erased, and this is apparent in Fig. 3. The most dense regions lose substructure within 1 Myr (panel a), the medium density regions lose substructure within 5 Myr (panel b) and the low

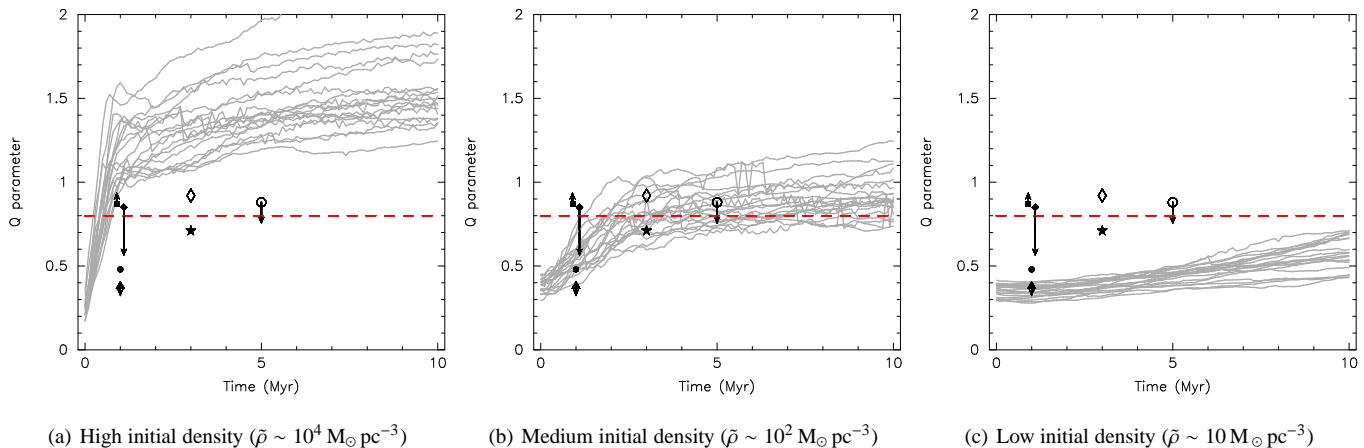
density regions retain substructure for the duration of the simulations (panel c). Given the high initial densities in Fig. 3(a), only the ONC is consistent with very dense initial conditions. When the initial conditions are a factor of ~ 100 less dense, the measured Q -parameters for every region apart from the ONC are consistent with more quiescent, medium density initial conditions for star formation.

3.3 The $Q - \Sigma_{\text{LDR}}$ plot

Finally, we present the $Q - \Sigma_{\text{LDR}}$ plot (Parker et al. 2014) for our simulations in Fig. 4. This combines the Q -parameter with the ratio of the median surface density of the 10 most massive stars compared to the median surface density of the region as a whole (Maschberger & Clarke 2011);

$$\Sigma_{\text{LDR}} = \frac{\bar{\Sigma}_{10}}{\bar{\Sigma}_{\text{all}}}. \quad (5)$$

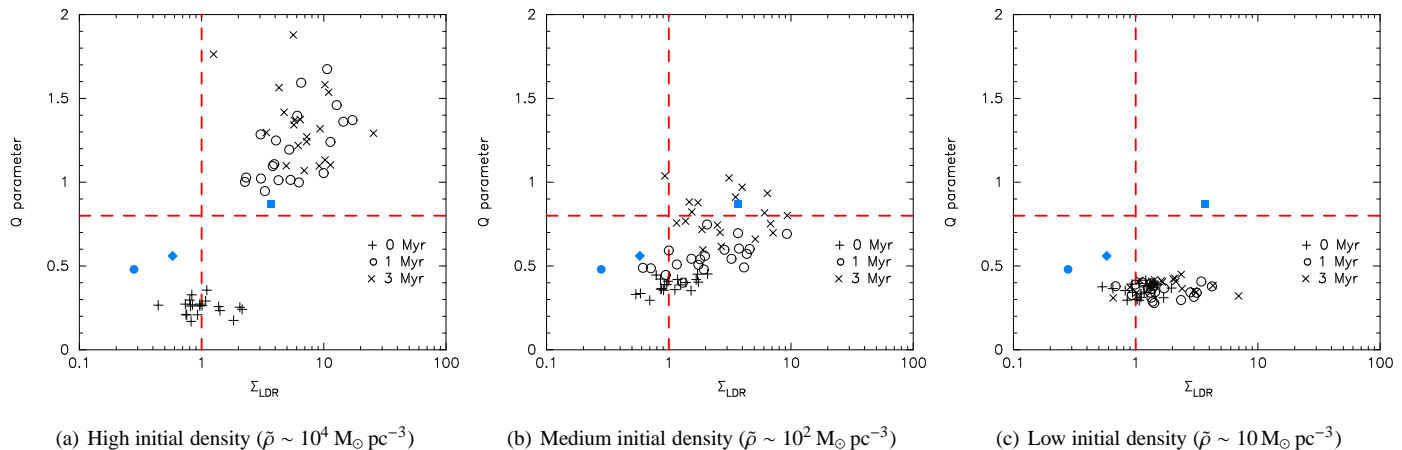
In Fig. 4 we show the datapoints for Taurus (filled circle), ρ Oph (filled diamond) and the ONC (filled square). These are the only


 (a) High initial density ($\bar{\rho} \sim 10^4 M_{\odot} \text{pc}^{-3}$)

 (b) Medium initial density ($\bar{\rho} \sim 10^2 M_{\odot} \text{pc}^{-3}$)

 (c) Low initial density ($\bar{\rho} \sim 10 M_{\odot} \text{pc}^{-3}$)

Figure 3. Evolution of structure as measured by the Q -parameter in our simulated star-forming regions. In panel (a) the star-forming regions have high initial densities ($\bar{\rho} \sim 10^4 M_{\odot} \text{pc}^{-3}$), in panel (b) the regions have medium initial densities ($\bar{\rho} \sim 10^2 M_{\odot} \text{pc}^{-3}$) and in panel (c) the regions have much lower initial densities ($\bar{\rho} \sim 10 M_{\odot} \text{pc}^{-3}$). We show the evolution of the Q -parameter in each simulation by the individual grey (solid) lines. The boundary between substructured regions and centrally concentrated regions at $Q = 0.8$ is shown by the horizontal dashed line. The Q -parameters measured in the star-forming regions of interest are shown by the points at 1, 3 and 5 Myr, depending on the age of the region. Where there is an uncertainty associated with the measurement of Q , we draw an arrow in the direction to indicate the possible deviation from the measured value. A key to the symbols is provided in Table 1


 (a) High initial density ($\bar{\rho} \sim 10^4 M_{\odot} \text{pc}^{-3}$)

 (b) Medium initial density ($\bar{\rho} \sim 10^2 M_{\odot} \text{pc}^{-3}$)

 (c) Low initial density ($\bar{\rho} \sim 10 M_{\odot} \text{pc}^{-3}$)

Figure 4. Evolution of structure as measured by the Q -parameter in our simulated star-forming regions versus the relative local density around massive stars compared to the region's median (Σ_{LDR}). We show values at 0 Myr (plus signs), 1 Myr (open circles) and 3 Myr (crosses). We show the observed values for Taurus (the filled circle), ρ Oph (the filled diamond) and the ONC (the filled square). In panel (a) the star-forming regions have high initial densities ($\bar{\rho} \sim 10^4 M_{\odot} \text{pc}^{-3}$), in panel (b) the regions have medium initial densities ($\bar{\rho} \sim 10^2 M_{\odot} \text{pc}^{-3}$) and in panel (c) the regions have much lower initial densities ($\bar{\rho} \sim 10 M_{\odot} \text{pc}^{-3}$). The boundary between substructured regions and centrally concentrated regions at $Q = 0.8$ is shown by the horizontal dashed line, and $\Sigma_{\text{LDR}} = 1$ (where the median local density around massive stars is equal to the region median) is shown by the vertical dashed line.

regions in our sample for which we have a reliable census with mass estimates for each individual star in order to determine Σ_{LDR} .

Under the reasonable assumption that the velocities of stars are correlated on local scales (Larson 1982), Parker et al. (2014) showed that massive stars attain higher surface densities than the median in the region, because they act as potential wells and acquire a retinue of low-mass stars. In the high density simulated regions (Fig. 4(a)), all of the simulations develop high Σ_{LDR} values in addition to erasing the primordial substructure. The only observed region which is consistent with these initial conditions is the ONC, and this appears to be marginal. The other observed regions (Taurus and ρ Oph) are more consistent with a much lower initial density, as they have $\Sigma_{\text{LDR}} < 1$ and $Q < 0.8$.

3.4 Discussion of individual regions

Recently, King et al. (2012b) claimed that differences between the binary separation distributions in nearby star-forming regions were likely to be primordial, as the main differences between binary populations in some regions and the corresponding separation range in the Galactic field were in the ‘hard’ binary regime (< 100 au), and thus unlikely to be the result of dynamical evolution. However, Marks et al. (2014) show that when the binary fraction is also considered, all of the regions discussed in King et al. (2012b) are in fact consistent with the dynamical evolution of a common binary population and the observed differences between regions are likely due to those regions having different initial densities. Here, we combine the results shown in Figs. 2, 3 and 4 to determine the likely initial (or maximum) density of each region in Table 1 (the

star forming regions presented in King et al. 2012b), and whether this density is consistent with dynamical processing of the universal initial binary population, as suggested by Marks & Kroupa (2012) and Marks et al. (2014). We summarise the results in Table 2.

ONC: The ONC has both a high Q -parameter and Σ_{LDR} ratio, which suggests that its initial density was likely $\bar{\rho} \sim 10^4 M_{\odot} \text{pc}^{-3}$. However, if its density were higher, the Q -parameter would also be higher, so $10^4 M_{\odot} \text{pc}^{-3}$ is very much an upper limit on the initial density. Marks & Kroupa (2012) suggest an initial density of $68\,000 M_{\odot} \text{pc}^{-3}$, with values lower than $46\,000 M_{\odot} \text{pc}^{-3}$ or higher than $90\,000 M_{\odot} \text{pc}^{-3}$ excluded with 90 per cent confidence. However, we note that the evolution of the universal binary population in our regions does appear to be consistent with the data from Reipurth et al. (2007) – compare the solid histogram with the squares in Fig. 1.

ρ **Oph:** If we take $Q = 0.56$ (Alves de Oliveira et al. 2012; Parker et al. 2012) for ρ Oph, with $\Sigma_{\text{LDR}} = 0.58$ then this is consistent with a moderate initial density ($10^2 - 10^3 M_{\odot} \text{pc}^{-3}$), rather than high initial (or maximum densities). Marks & Kroupa (2012) suggest an initial density of $2300 M_{\odot} \text{pc}^{-3}$, with values lower than $1100 M_{\odot} \text{pc}^{-3}$ or higher than $7400 M_{\odot} \text{pc}^{-3}$ excluded with 90 per cent confidence. One of our medium density simulations briefly reaches a density of $2000 M_{\odot} \text{pc}^{-3}$, suggesting that the evolution of this region (and processing of binaries) could be consistent with the universal initial binary population.

Taurus: The low Q -parameter (0.48 – Cartwright & Whitworth 2004) and low Σ_{LDR} (0.28 using the dataset from Parker et al. 2011) suggest that dynamical evolution has not been significant in this region. Taurus is consistent with very quiescent initial conditions ($\rho \sim 10 M_{\odot} \text{pc}^{-3}$ – Figs. 2(c) and 3(c)). Marks & Kroupa (2012) suggest an initial density of $350 M_{\odot} \text{pc}^{-3}$, with values lower than $140 M_{\odot} \text{pc}^{-3}$ or higher than $850 M_{\odot} \text{pc}^{-3}$ excluded with 90 per cent confidence. Given its current low density, low Q -parameter and low Σ_{LDR} , Taurus is not consistent with the universal initial binary population.

IC 348: Because of its age (3 Myr), if IC 348 had initially high density, two-body relaxation would have reduced the density to values much lower than observed for this region (see Fig. 2). This, combined with the Q -parameter of 0.92 (Cartwright & Whitworth 2004) suggests a moderate initial density ($10^2 - 10^3 M_{\odot} \text{pc}^{-3}$ – see panel (b) of Figs. 2 and 3). Marks & Kroupa (2012) suggest an initial density of $9400 M_{\odot} \text{pc}^{-3}$, with values lower than $2700 M_{\odot} \text{pc}^{-3}$ or higher than $53\,000 M_{\odot} \text{pc}^{-3}$ excluded with 90 per cent confidence. Such a high initial density is inconsistent with the observed structure and current density, and its binary population is probably not evolved from the Kroupa (1995b) universal binary population.

Cham I: Chamaeleon I has an age of 3 Myr, and a low density, but relatively high Q -parameter of 0.71 (Cartwright & Whitworth 2009). Figs. 2 and 3 show that none of our dynamical scenarios fit the observed values, and it is therefore likely that Cham I formed with its current density and structure – and that dynamical evolution has not altered its binary population. Marks & Kroupa (2012) suggest an initial density of $1600 M_{\odot} \text{pc}^{-3}$, with values lower than $230 M_{\odot} \text{pc}^{-3}$ or higher than $13\,000 M_{\odot} \text{pc}^{-3}$ excluded with 90 per cent confidence. Given its current low density and lack of dynamical evolution, Cham I is not consistent with the universal binary population.

CrA: CrA has $Q = 0.38$ but a moderate density of $30 M_{\odot} \text{pc}^{-3}$ (Neuhäuser & Forbrich 2008; King et al. 2012b). According to our evolutionary models, CrA could have evolved slightly from a highly substructured region with an initial density of $\sim 10^2 M_{\odot} \text{pc}^{-3}$. In order to be consistent with the initial universal

binary population, Marks et al. (2014) suggest an initial density of $190 M_{\odot} \text{pc}^{-3}$ (without providing limits). Our analysis suggests that this region is consistent with the universal initial binary population, assuming a similar magnitude in the confidence limit range as for the other regions.

Upper Sco: The Q -parameter is 0.88 (Kraus & Hillenbrand 2007) and current density is $16 M_{\odot} \text{pc}^{-3}$ (King et al. 2012b); both of which imply that Upper Sco is likely to have had moderately dense initial conditions ($\rho \sim 10^2 - 10^3 M_{\odot} \text{pc}^{-3}$). Marks et al. (2014) suggest an initial density of $4200 M_{\odot} \text{pc}^{-3}$ (again without confidence limits). Our evolutionary models suggest that Upper Sco is also inconsistent with the initial densities required to process the universal initial binary population.

In summary, only ρ Oph, CrA, and possibly the ONC, are consistent with the dynamical processing of the universal initial binary population from Kroupa (1995a,b), based on the consideration of the regions' structure and current density. We suggest that the observed differences between these regions are likely to be a relic of the star formation process, although we caution that as the binaries observed in these regions are 'intermediate' they may still have undergone some degree of dynamical evolution (Parker & Goodwin 2012).

4 CONCLUSIONS

We have presented N -body simulations of the dynamical evolution of star-forming regions in which we follow the stellar density and spatial structure and compare the results to seven observed regions. For each individual region, we determine the likely initial density (which is usually, but not always, the maximum) based on its observed current density and spatial structure, as determined by the Q -parameter.

The spatial structure of a region is a strong constraint on the amount of dynamical evolution that has taken place, as dense regions $\bar{\rho} > 10^3 M_{\odot} \text{pc}^{-3}$ erase structure almost immediately, intermediate density regions ($\bar{\rho} \sim 10^2 - 10^3 M_{\odot} \text{pc}^{-3}$) remove structure within 5 Myr but low-density regions ($\bar{\rho} < 10 M_{\odot} \text{pc}^{-3}$) retain structure beyond the age of all of the regions considered here. Folding in the measurement of structure largely removes the density degeneracy problem in star formation, where the initial density is very difficult to constrain due to the rapid expansion of initially dense regions, and the slower expansion of more quiescent regions, both of which can result in the same present-day density from very different initial conditions.

Our results can be used to infer the likely maximum density of observed star-forming regions, which for example enables the importance of the effects of dynamical interactions and radiation from massive stars on protoplanetary discs to be ascertained (e.g. Scally & Clarke 2001; Adams et al. 2006; Rosotti et al. 2014). Recently, de Juan Ovelar et al. (2012) showed an apparent dependence of the size of protoplanetary discs on the density of the star-forming environment, although their observations were limited to nearby star-forming regions. Future ALMA observations may be able to probe discs in more distant regions (e.g. Mann et al. 2014), and using the Q -parameter in tandem with the present-day density will be useful in determining whether any observed trends in disc size are due to the star-formation environment.

We also apply our method to determine which of seven nearby star-forming regions are consistent with the 'universal initial binary population' model for star formation (Kroupa 1995a,b),

Table 2. Comparison of the structure and density of seven star-forming regions with N -body simulations to determine which are compatible with the universal initial binary population from Kroupa (1995a,b). From left to right, the columns show the region name, age, Q -parameter (where two values are given due to observational uncertainty, the arrow indicates the more likely value), the observed present-day density of each region as noted by Marks & Kroupa (2012) and King et al. (2012b), $\rho_{\text{obs.}}$, the postulated initial density with upper and lower limits from Marks & Kroupa (2012) and Marks et al. (2014) for the binary population of that region to be consistent with the universal primordial binary properties (Kroupa 1995a,b), $\rho_{\text{post.}}$, the maximum possible initial density when the Q -parameter is also considered, $\rho_{\text{max.}}$, and whether or not this region is consistent with the Kroupa (1995a,b) universal initial binary population.

Region	Age	Q	$\rho_{\text{obs.}}$	$\rho_{\text{post.}}$	$\rho_{\text{max.}}$	Universal population?
ONC	1 Myr	0.87 \rightarrow 0.94	400 $M_{\odot} \text{pc}^{-3}$	68 000 $^{+90\,000}_{-46\,000}$ $M_{\odot} \text{pc}^{-3}$	10 000 $M_{\odot} \text{pc}^{-3}$	no ^a
ρ Oph	1 Myr	0.56 \leftarrow 0.85	200 $M_{\odot} \text{pc}^{-3}$	2300 $^{+7400}_{-1100}$ $M_{\odot} \text{pc}^{-3}$	2000 $M_{\odot} \text{pc}^{-3}$	yes
Taurus	1 Myr	0.48	8 $M_{\odot} \text{pc}^{-3}$	350 $^{+850}_{-140}$ $M_{\odot} \text{pc}^{-3}$	10 $M_{\odot} \text{pc}^{-3}$	no
IC 348	3 Myr	0.92	180 $M_{\odot} \text{pc}^{-3}$	9400 $^{+53\,000}_{-2700}$ $M_{\odot} \text{pc}^{-3}$	1000 $M_{\odot} \text{pc}^{-3}$	no
Cham I	3 Myr	0.66 \rightarrow 0.71	1 $M_{\odot} \text{pc}^{-3}$	1600 $^{+13\,000}_{-230}$ $M_{\odot} \text{pc}^{-3}$	1 $M_{\odot} \text{pc}^{-3}$	no
CrA	1 Myr	0.32 \leftarrow 0.38	30 $M_{\odot} \text{pc}^{-3}$	190 $M_{\odot} \text{pc}^{-3}$	100 $M_{\odot} \text{pc}^{-3}$	yes
Upper Sco	5 Myr	0.75 \leftarrow 0.88	16 $M_{\odot} \text{pc}^{-3}$	4200 $M_{\odot} \text{pc}^{-3}$	1000 $M_{\odot} \text{pc}^{-3}$	no

^aNote that an initial density of $10^4 M_{\odot} \text{pc}^{-3}$ for the ONC appears to be consistent with the universal binary population in Fig. 1. However, this (relatively low) density was ruled out at 90 per cent confidence by Marks & Kroupa (2012).

based on recent numerical simulations presented in the literature (Marks & Kroupa 2012; Marks et al. 2014). We compare the density of our simulations which fit the observed regions' structure and determine whether the initial density of those simulations is high enough to process the initial binary population to resemble the binary properties observed in each region today, using the values quoted in Marks & Kroupa (2012) and Marks et al. (2014). We find that of the seven regions observed, only three – ρ Oph, CrA and possibly the ONC – are consistent with the universal initial binary population model for star formation.

Unfortunately, aside from discarding the universal initial binary population hypothesis in Kroupa (1995a,b), our results do not help much in assessing the type of star-forming region that contributes binaries to the Galactic field. We are still limited by the observed separation range in regions (10s – 1000s au) which is small compared to the field (10^{-2} – 10^5 au), and by the fact that these visual binaries are dynamically 'intermediate' systems (Heggie 1975; Hills 1975a,b) that could have evolved stochastically (especially in dense regions like the ONC, Parker & Goodwin 2012). We also have very little information on whether the regions considered are representative of those that do populate the field. Further observations of e.g. spectroscopic binaries which are not affected by dynamical evolution are desperately required in order to look for stark differences between the binary populations of the regions in question and the Galactic field.

ACKNOWLEDGEMENTS

I am grateful to the referee, Cathie Clarke, for her comments and suggestions which have led to a more interesting paper. I acknowledge support from the Royal Astronomical Society in the form of a research fellowship.

REFERENCES

- Adams F. C., 2011, *ARA&A*, 48, 47
 Adams F. C., Proszkow E. M., Fatuzzo M., Myers P. C., 2006, *ApJ*, 641, 504
 Alexander R., Pascucci I., Andrews S., Armitage P., Cieza L., 2013, arXiv: 1311.1819
 Allison R. J., Goodwin S. P., Parker R. J., Portegies Zwart S. F., de Grijs R., 2010, *MNRAS*, 407, 1098
 Alves de Oliveira C., Moraux E., Bouvier J., Bouy H., 2012, *A&A*, 539, A151
 André P., Men'shchikov A., Bontemps S., Könyves V., Motte F., Schneider N., Didelon P., Minier V., Saraceno P., Ward-Thompson D., et al. 2010, *A&A*, 518, L102
 Armitage P. J., 2000, *A&A*, 362, 968
 Bastian N., Gieles M., Ercolano B., Gutermuth R., 2009, *MNRAS*, 392, 868
 Bonnell I. A., Bate M. R., Clarke C. J., Pringle J. E., 2001, *MNRAS*, 323, 785
 Bressert E., Bastian N., Gutermuth R., Megeath S. T., Allen L., Evans, II N. J., Rebull L. M., Hatchell J., Johnstone D., Bourke T. L., Cieza L. A., Harvey P. M., Merin B., Ray T. P., Tothill N. F. H., 2010, *MNRAS*, 409, L54
 Cartwright A., 2009, *MNRAS*, 400, 1427
 Cartwright A., Whitworth A. P., 2004, *MNRAS*, 348, 589
 Cartwright A., Whitworth A. P., 2009, *MNRAS*, 392, 341
 Dale J. E., Ercolano B., Bonnell I. A., 2013, *MNRAS*, 430, 234
 Davies M. B., Adams F. C., Armitage P., Chambers J., Ford E., Morbidelli A., Raymond S. N., Veras D., 2013, arXiv: 1311.6816
 de Juan Ovelar M., Kruijssen J., Bressert E., Testi L., Bastian N., Cánovas Cabrera H., 2012, *A&A*, 546, L1
 Duchêne G., Kraus A., 2013, *ARA&A*, 51, 269
 Duquennoy A., Mayor M., 1991, *A&A*, 248, 485
 Fischer D. A., Marcy G. W., 1992, *ApJ*, 396, 178
 Gieles M., Moeckel N., Clarke C. J., 2012, *MNRAS*, 426, L11
 Girichidis P., Federrath C., Allison R., Banerjee R., Klessen R. S., 2012, *MNRAS*, 420, 3264
 Goodwin S. P., 2010, *Royal Society of London Philosophical Transactions Series A*, 368, 851
 Goodwin S. P., Whitworth A. P., 2004, *A&A*, 413, 929
 Gouliermis D. A., Hony S., Klessen R. S., 2014, *MNRAS*, 439, 3775
 Heggie D. C., 1975, *MNRAS*, 173, 729
 Hillenbrand L. A., Hartmann L. W., 1998, *ApJ*, 492, 540
 Hills J. G., 1975a, *AJ*, 80, 809

- Hills J. G., 1975b, *AJ*, 80, 1075
- King R. R., Parker R. J., Patience J., Goodwin S. P., 2012a, *MNRAS*, 421, 2025
- King R. R., Goodwin S. P., Parker R. J., Patience J., 2012b, *MNRAS*, 427, 2636
- Köhler R., Leinert C., 1998, *A&A*, 331, 977
- Kraus A. L., Hillenbrand L. A., 2007, *ApJ*, 662, 413
- Kroupa P., 1995a, *MNRAS*, 277, 1491
- Kroupa P., 1995b, *MNRAS*, 277, 1507
- Kroupa P., 1995c, *MNRAS*, 277, 1522
- Kroupa P., 2002, *Science*, 295, 82
- Kroupa P., Petr M. G., McCaughrean M. J., 1999, *New Astronomy*, 4, 495
- Kroupa P., Petr-Gotzens M. G., 2011, *A&A*, 529, A92
- Lada C. J., 2010, *Royal Society of London Philosophical Transactions Series A*, 368, 713
- Lada C. J., Lada E. A., 2003, *ARA&A*, 41, 57
- Larson R. B., 1982, *MNRAS*, 200, 159
- Leinert C., Zinnecker H., Weitzel N., Christou J., Ridgway S. T., Jameson R., Haas M., Lenzen R., 1993, *A&A*, 278, 129
- Mann R. K., Di Francesco J., Johnstone D., Andrews S. M., Williams J. P., Bally J., Ricci L., Hughes A. M., Matthews B. C., 2014, *ApJ*, 784, 82
- Marks M., Kroupa P., 2012, *A&A*, 543, A8
- Marks M., Leigh N., Giersz M., Pfalzner S., Pflamm-Altenburg J., Oh S., 2014, *MNRAS*, 441, 3503
- Maschberger T., Clarke C. J., 2011, *MNRAS*, 416, 541
- Mathieu R. D., 1994, *ARA&A*, 32, 465
- Metchev S. A., Hillenbrand L. A., 2009, *ApJS*, 181, 62
- Moeckel N., Holland C., Clarke C. J., Bonnell I. A., 2012, *MNRAS*, 425, 450
- Neuhäuser R., Forbrich J., 2008, *The Corona Australis Star Forming Region*. p. 735
- Olczak C., Pfalzner S., Eckart A., 2008, *A&A*, 488, 191
- Parker R. J., Bouvier J., Goodwin S. P., Moraux E., Allison R. J., Guieu S., Güdel M., 2011, *MNRAS*, 412, 2489
- Parker R. J., Goodwin S. P., 2012, *MNRAS*, 424, 272
- Parker R. J., Maschberger T., Alves de Oliveira C., 2012, *MNRAS*, 426, 3079
- Parker R. J., Meyer M. R., 2012, *MNRAS*, 427, 637
- Parker R. J., Quanz S. P., 2012, *MNRAS*, 419, 2448
- Parker R. J., Wright N. J., Goodwin S. P., Meyer M. R., 2014, *MNRAS*, 438, 620
- Pecaut M. J., Mamajek E. E., Bubar E. J., 2012, *ApJ*, 746, 154
- Portegies Zwart S. F., McMillan S. L. W., Hut P., Makino J., 2001, *MNRAS*, 321, 199
- Portegies Zwart S. F., Makino J., McMillan S. L. W., Hut P., 1999, *A&A*, 348, 117
- Raghavan D., McMaster H. A., Henry T. J., Latham D. W., Marcy G. W., Mason B. D., Gies D. R., White R. J., ten Brummelaar T. A., 2010, *ApJSS*, 190, 1
- Reggiani M. M., Meyer M. R., 2013, *A&A*, 553, A124
- Reipurth B., Guimarães M. M., Connelley M. S., Bally J., 2007, *AJ*, 134, 2272
- Rosotti G. P., Dale J. E., de Juan Ovelar M., Hubber D. A., Kruijssen J. M. D., Ercolano B., Walch S., 2014, *MNRAS*, 441, 2094
- Sánchez N., Alfaro E. J., 2009, *ApJ*, 696, 2086
- Scally A., Clarke C., 2001, *MNRAS*, 325, 449
- Schmeja S., Klessen R. S., 2006, *A&A*, 449, 151
- Shu F. H., Adams F. C., Lizano S., 1987, *ARA&A*, 25, 23